Fast piezoelectric valve offering controlled gas injection in magnetically confined fusion plasmas for diagnostic and fuelling purposes

M. Griener,[1, 2, a)] O. Schmitz,[3] K. Bald,[1] D. Bösser,[1] M. Cavedon,[1] P. De Marné,[1] T. Eich,[1] G. Fuchert,[4] A. Herrmann,[1] A. Kappatou,[1] T. Lunt,[1] V. Rohde,[1] B. Schweer,[5] M. Sochor,[1] U. Stroth,[1, 2] A. Terra,[5] E. Wolfrum,[1] and the ASDEX Upgrade Team[1]

[1)] *Max Planck Institute for Plasma Physics, Boltzmannstr. 2, 85748 Garching, Germany*

[2)] *Physik Department E28, Technische Universität München, 85748 Garching, Germany*

[3)] *Department of Engineering Physics, University of Wisconsin-Madison, USA*

[4)] *Max Planck Institute for Plasma Physics, Wendelsteinstr. 1, 17491 Greifswald, Germany*

[5)] *FZ Jülich, Institute for Energy- and Climate Research, 52428 Jülich, Germany*

(Dated: 22 September 2016)

In magnetically confined fusion plasmas controlled gas injection is crucial for plasma fuelling as well as for various diagnostic applications such as active spectroscopy.
We present a new, versatile system for the injection of collimated thermal gas beams into a vacuum chamber. This system consists of a gas pressure chamber, sealed by a custom made piezo valve towards a small capillary for gas injection. The setup can directly be placed inside of the vacuum chamber of fusion devices as it is small and immune against high magnetic fields. This enables gas injection close to the plasma periphery with high duty cycles and fast switch on/off times $\lesssim 0.5\,\mathrm{ms}$.
In this work, we present the design details of this new injection system and a systematic characterization of the beam properties as well as the gas flowrates which can be accomplished. The thin and relatively short capillary yields a small divergence of the injected beam with a half opening angle of 20 deg. The gas box is designed for pre-fill pressures of 10 mbar up to 100 bar and makes a flowrate accessible from 10^{18} part/s up to 10^{23} part/s. It hence is a versatile system for both, diagnostic as well as fuelling applications. The implementation of this system in ASDEX Upgrade (AUG) will be described and its application for line ratio spectroscopy on helium will be demonstrated on a selected example.

Keywords: fusion, plasma, scrape-off-layer, piezo valve, gas injection, plasma fuelling, active spectroscopy, helium line ratio spectroscopy, gas-puff imaging

[a)]Electronic mail: michael.griener@ipp.mpg.de

I. INTRODUCTION

In devices for magnetic confinement of fusion plasmas as tokamaks or stellerators as well as linear machines, controlled gas injection is crucial for plasma fuelling and diagnostic applications. Special piezo based valves offer fast response and switching times for a wide range of applications. Typically valves are placed far away from the plasma periphery as the systems are not constructed to withstand the harsh environment of strong magnetic fields and high thermal loads. The resulting dead volume in the vacuum system and the pipe conductance leads to long response times of the gas flux, also the valves itself provides faster responses[1].

Therefore several specialised systems for different application have been developed to compensate this disadvantage. A spring driven piezoelectric valve[2] for disruption mitigation enables the injection of high amounts of gases in a short time.

A supersonic piezo based gas valve[3] has been used in TEXTOR for line ratio spectroscopy on helium[4]. However, while the supersonic system is very involved in terms of setup and maintenance, desire exists for simpler but still flexible valves for both, fuelling and diagnostic applications. Such a versatile piezo valve system for thermal gas beams is presented and characterised in this paper.

The valve can be placed inside the vacuum vessel close to the plasma periphery, compensating the higher divergence angle of the thermal beam compared to supersonic beams with a small distance of the gas injection point to the observation point. A thin and short capillary is used for gas injection. This has two major advantages. First, it yields a small divergence of the injected beam with a half opening angle of 20 deg. Second, it ensures a very fast response of the valve which enables fast chopping of gas beams. This had been shown to be a valuable technique for background subtraction as realised with the Lithium beam[5,6] and the charge exchange recombination spectroscopy (CXRS)[7] diagnostics at ASDEX Upgrade (AUG).

At ASDEX Upgrade the versatile piezo valve system is applied for helium line ratio spectroscopy as well as for gas-puff imaging (GPI)[8] which requires higher gas fluxes.

The valve properties are discussed part by part, in the paper which is organised as follows: In section II we present an overview and the design details of the piezo valve. In section III, the sealing mechanism and in section IV the gas supply system for the piezo valve is de-

scribed. In section V the physical basics of gas flows through a capillary are summarised. This leads to a prediction of the achievable flowrates. The flow measurements for different operation regimes are presented in section VI. In section VII the achievable switching times are presented, whereas measurements of the shape of the gas beam are presented in section VIII. This is important for the achievable spatial resolution of diagnostic applications. In section IX the suitability of the valve for diagnostic purposes in the scrape-off layer (SOL) region of AUG is shown for a selected example.

II. OVERVIEW AND DESIGN DETAILS OF THE PIEZO VALVE

The piezo electric valve is based on a modular concept of several custom made parts (stainless steel 1.4301, total mass $\sim 3\,\mathrm{kg}$, cf. Figure 1 and Figure 2). The central element is the commercially available piezo actor "PX 500"[9] (dimensions: $52 \times 20 \times 8\,\mathrm{mm}$) with a total stroke of 800 µm in a voltage range from $-20\,\mathrm{V}$ to $130\,\mathrm{V}$. It is directly placed in the gas pressure chamber with dimensions ($10 \times 7 \times 7\,\mathrm{cm}$) and a volume of $100\,\mathrm{cm}^3$. This gas chamber is connected to the ground plate with eight M6x20 screws and sealed with a HELICOFLEX[10] metal sealing. This enables, as stress calculations for leak tests show, filling pressures up to 100 bar.

To adjust the gas flowrate, variable pressures (tested from 10 mbar up to 7 bar) can be applied using the gas supply system which is described in section IV. This enables the tuning of the gas flux at fully opened valve over a wide range in a precise way (cf. Section VI).

For a fully opened valve the gas flow is only limited by the diameter and length of the capillary used for gas supply. According to the application of the valve, different diameters can be used. Capillaries with a length of 66 mm and diameters of 400 µm and 700 µm had been tested for diagnostic purpose.

The gas pressure chamber is sealed (see also section III) towards the capillary by a Viton plate pressed on a truncated cone with an orifice of 400 µm diameter in the middle. The sealing area is around $1\,\mathrm{mm}^2$ with a contact pressure force at closed valve (0 V piezo voltage) of 3 N. For a fully opened valve the Viton plate is lifted by 500 µm.

The operation temperature of the valve is restricted by the piezo actor between $-20\,^\circ\mathrm{C}$ and $80\,^\circ\mathrm{C}$. In this range the maximal piezo stroke is temperature dependent (cf. Section VI C). Therefore the temperature is measured with a Pt100 sensor. For baking the vacuum chamber

of AUG, temperatures of 150 °C are required. This is possible while the piezo is not operated. The gas as well as the electric supply for the piezo actor and the thermo element is provided through the pipe for gas supply. A 4-pin LEMO[11] connector with a custom made case connects the electrical parts when the gas box is closed.

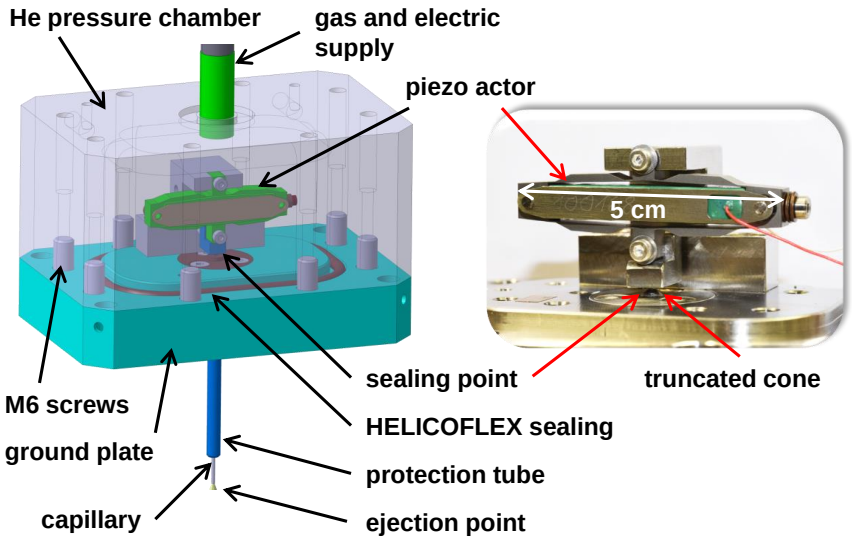

FIG. 1: CAD drawing (left) and photo (right) of the piezo valve. A cross section view is presented in Figure 2.

III. SEALING MECHANISM

Figure 2 shows a cross section view of the valve, representing the connection of the capillary to the gas pressure box and the sealing mechanism. Two different concepts for the sealing mechanism are presented in Figure 3. Both are based on a Viton part pressed on a 400 µm perforation in the sealing plate (cf. (3) in Figure 2). The capillary diameter can thus be chosen arbitrarily, dependent on the application of the valve. For high gas fluxes at low pressures (e.g. $> 1.6 \times 10^{21}$ particles/second at 1 bar pressure) also the diameter at the sealing point has to be enlarged thus it becomes the flux limiting part (cf. Section V B). The design with the thin and short capillary attached to the sealing plate minimises the enclosed volume between the sealing and gas ejection point ($\sim 9\,\mathrm{mm}^3$). This leads to fast formation and decay times of the gas beam (cf. Section VII), which is one of the main advantages of the system presented here, compared to conventional valve systems

which are placed further away from the plasma. Before we describe the valve performance characteristics, the optimisation of the actual sealing mechanism, covering two different approaches, is discussed in the next section.

A. Comparison of the sealing mechanisms

The first approach (cf. Figure 3 a)) is based on a cylindrical Viton plug (2 mm diameter, 5 mm total length) pressed on an orifice with a diameter of 400 µm. The Viton plug is mechanically fixed in a perforated bracket.

The second approach shown in Figure 3 b) is based on a Viton plate (5 mm diameter, 1 mm thickness) pressed on a perforated truncated cone. This technique has several advantages compared to the first one.

On the one hand it is more tolerant against temperature changes. The reason for this is that the thermal expansion of Viton ($\sim 250 \times 10^{-6}\,\mathrm{K}^{-1}$) is about 25 times higher compared to stainless steel. The resulting length increase of of the Viton plug in approach a) hinders the full opening of the valve for temperatures higher than 60 °C.

On the other hand, the Viton plate is stiffer than the Viton plug. The flexibility of the plug leads to a barrel shaped deformation of the plug when the valve is closed. When the valve is opened this shape is preserved before the Viton plug relaxes. This is shown in Figure 4 where the barrel formation is demonstrated during an opening sequences from closed (left figure) to open (middle figure) and to open piezo position with relaxed Viton plug (right). The lower row shows a sketch and the upper row photographs of the Viton plug behaviour. This effect can lead to a resealing of the valve if the piezo movement is smaller than the deformation Δx of the Viton plug. The relaxation time of the plug is strongly temperature dependent. At a temperature of 5 °C the relaxation takes several seconds. At 25 °C full relaxation needs around 0.9 s whereas at 80 °C the relaxation is completed within 30 ms.

Furthermore, the higher stiffness of the Viton plate has two additional consequences: The first one is that a smaller deformation Δx is needed to achieve the same initial tension compared to the Viton plug, increasing the final displacement of the piezo from 400 µm to about 500 µm. The achieved higher clearance removes the influence of oscillations occurring during the opening process (cf. Section VII).

The second consequence is that the stiffer system needs a smaller movement of the piezo for

a full opening of the valve. This leads to a smaller required voltage change and thus to a faster switching time (cf. Section VI A).

Therefore the approach with the Viton plate is used for the valve system at ASDEX Upgrade.

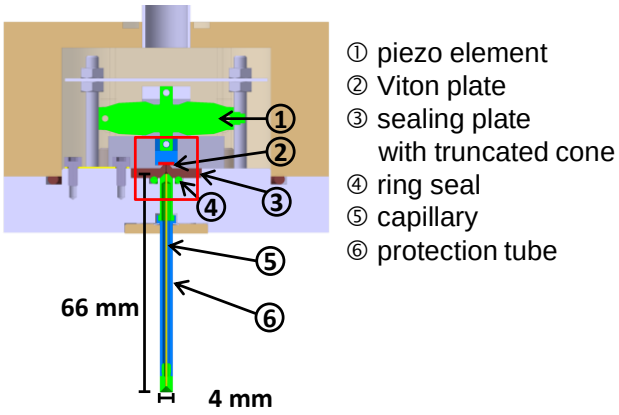

FIG. 2: Cross section of the valve. The magnification of the red square is presented in Figure 3.

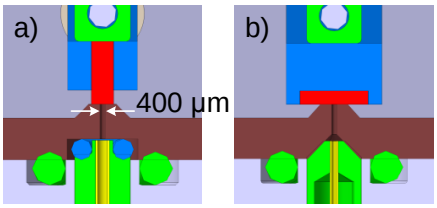

FIG. 3: Comparison of two different sealing mechanisms a) Viton plug, b) Viton plate to seal the 400 µm orifice.

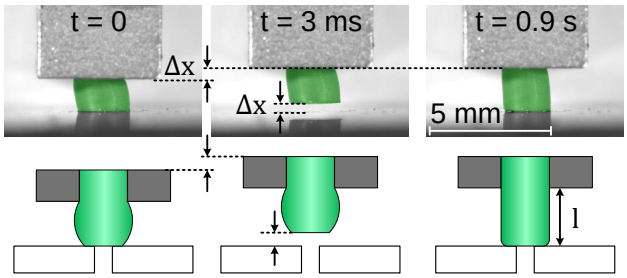

FIG. 4: Real images (top) and schematic drawings (bottom) of the Viton plug for a closed piezo (left) and an opened piezo after 3 ms (middle) and 900 ms (right). The images (upper row) had been recorded with the fast camera "Phantom v711".

IV. GAS SUPPLY SYSTEM

Figure 5 illustrates the gas supply circuit for the piezo valve system (blue) as well as the setup for the gas flux (cf. Section VI) and beam shape (cf. Section VIII) lab measurements (red).

To measure the mean gas flowrate through the piezo valve, the valve is placed in a vacuum chamber. The valve is supplied by a gas system, which allows the regulation of the pressure in a precise way:

The gas from the gas bottle R1 is throttled by the valve TV1 to fill the gas reservoirs R2 and R3 if the pneumatic inlet valves V1 and V2 are open. The pressure in the system can be measured by the piezoresistive pressure sensor S1 in the range of $(1-1000)$ mbar and S2 in the range of $(1-20)$ bar.

Absolute system pressures higher than one bar can be reduced slowly through the throttle valve TV2 by opening the valve V5 or fast by opening the valve V4. Low pressures can be achieved by opening the valve V3, which leads to the vacuum pump DSP 2. Low pressures can be measured with the vacuum gauge S3.

The laboratory vacuum chamber is pumped with the turbomolecular pump TMP 1 which itself is connected to the rotary vane pump DSP 1. To measure the pressure rise in the chamber after gas injection with a baratron S4, the valve VC1 is closed before the gas pulse. The initial pressure in the vacuum chamber with a volume of (491 ± 5) l is around 1×10^{-7} mbar.

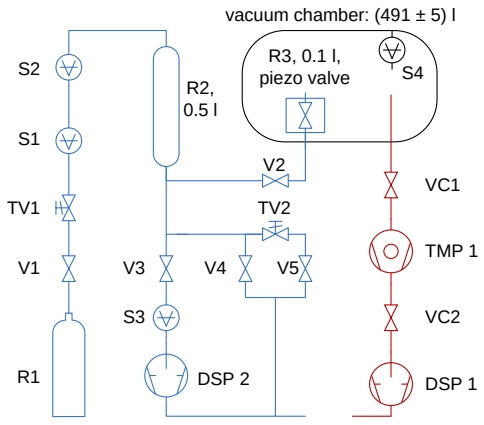

FIG. 5: Scheme of the gas supply circuit for the piezo valve (blue, left) and vacuum chamber pumping system (red, right) used for the lab measurements.

V. FLOWRATES

To calculate the mean gas flowrate during the gas pulse or the gas pulses, the ideal gas equation

$$pV = Nk_BT \tag{1}$$

is used, where p is the pressure in the volume V, T is the temperature, N is the number of gas particles and $k_B = 1.38 \times 10^{-23}\,\mathrm{J/K}$ is the Boltzmann constant. Because the number of injected particles is at least three orders of magnitude higher than the initial number of particles in the vacuum chamber, the initial pressure in the vacuum chamber can be approximated to be zero. Thus the number of injected particles is given by

$$N = \frac{\Delta p \cdot V}{k_BT}. \tag{2}$$

To achieve comparable results, the particle flowrate (particles per second, pps) is used in the following.

A. Flow regimes

Because the gas box is operated at pressures across $2-3$ orders of magnitude and different orifice openings as well as tube diameters, the actual flow rate depends on the flow regime obtained. To describe gas flowrates, different equations are valid depending on the gas pressure as well as the size of the orifice or tube through which the gas is expanding.
Concerning this, an important parameter is the mean free path of particles in a gas, which is the average distance the particles can travel between two collisions. It is given by[12] (eq. (21.101))

$$\lambda = \frac{k_BT}{\sqrt{2} \cdot \pi \cdot p \cdot (2r)^2}, \tag{3}$$

where p is the gas pressure and r is the hard shell radius of the gas particle which is in the order of a few Å.
The Knudsen number Kn puts the mean free path length λ in relation to the characteristic length scale D of the system, e.g. the diameter of a tube:

$$\mathrm{Kn} = \frac{\lambda}{D}. \tag{4}$$

It is an indicator for the probability of particle-particle collisions compared to particle wall interactions. For $\mathrm{Kn} \ll 1$ fluid equations can be used to describe the viscous flow regime

where the mean free path of the particles is much smaller than the dimension of the system. For Kn $\gg 1$, the interaction between particles can be neglected compared to particle wall interactions. Here, the stochastic process of particles passing a barrier in form of an orifice or small tube has to be considered, leading to the concept of molecular flow. The intermediate regime is called Knudsen flow.

For the valve geometry presented here (nozzle diameter 400 µm) the Knudsen number is 3.4×10^{-4} for 1 bar pressure (mean free path for He is 1.2×10^{-7} m) and Kn = 0.034 for 10 mbar (mean free path for He is 1.2×10^{-5} m). In both cases the flow can be described using a fluid approach.
For a detailed analysis of the problem, compressible (in general all kinds of gases) and non compressible flow regimes (e.g. liquids or dilute gases with very low pressure differences) have to be distinguished.

In the non compressible case, the Hagen-Poiseuille equation[13] (p.237, eq. (8.31)) can be applied for a Newtonian fluid to describe the particle flux through a round pipe with radius r_p and length L_p:

$$\dot{N} = \frac{\pi \cdot r_p^4}{8\eta} \frac{p^2}{L_p \cdot k_B T}. \tag{5}$$

In section VI B it is shown that the particle flowrate exhibits this quadratic pressure dependence (cf. Figure 8) for low pressures and small capillary diameters. In this case, the capillary decreases the flowrate by friction which decreases the pressure gradient, making compressible effects less important. This region of laminar flow can be described using the Hagen-Poiseuille equation.
For higher pressures the flowrate changes into a linear function of the system pressure (cf. Figure 7) as compressible effects become important. Therefore, equations for compressible fluids are applied in the following.

B. Valve and friction limited flow

In the compressible case one first can calculate the flux through a valve without capillary. In this case, the gas flow is only limited by the minimal diameter of the orifice. The resulting flux with attached capillary cannot be higher than the maximal flux $\dot{N}_{\max}$ in this valve limited

case. It can be calculated with the nozzle equation (cf.[14] (Chapter 4) and[15] (eq. (1a)))

$$\dot{N}_{\max} = n_0 c_s A_v \left(\frac{\gamma+1}{2}\right)^{-\frac{\gamma+1}{2(\gamma-1)}}, \tag{6}$$

which describes the particle flux from a reservoir with density n_0 through an orifice with the diameter D_v into vacuum.

In Equation 6, $A_v = \pi D_v^2/4$ is the cross section area of the orifice and

$$c_s = \sqrt{\frac{\gamma\, p}{\varrho}} = \sqrt{\frac{\gamma\, k_B T}{m}} \tag{7}$$

is the adiabatic sound speed ($c_s = 1.02\,\mathrm{km/s}$ for helium at $300\,\mathrm{K}$), where ϱ is the mass density and γ is the specific heat ratio of the gas used.

Using the ideal gas equation to set $n_0 = p_0/(k_B T)$, Equation 6 changes to

$$\dot{N}_{\max} = p_0 \cdot \frac{\pi}{4\sqrt{k_B}} \cdot \frac{D_v^2}{\sqrt{T \cdot m}} \cdot \sqrt{\gamma} \cdot \left(\frac{\gamma+1}{2}\right)^{-\frac{\gamma+1}{2(\gamma-1)}}. \tag{8}$$

At constant temperature, this equation shows a liner dependence on the pressure. It can be used to describe the flux of compressible gases in the frictionless (valve limited) case for thermal and supersonic expansions as described in[16] (eq. (3.11), p. 32).

In the supersonic case the Mach number

$$M = \frac{u}{c_s}, \tag{9}$$

which is the quotient of the flow speed u and the adiabatic sound speed c_s has to be used to describe the gas flux. The Mach number also becomes important if a capillary is attached to the valve (cf.[15]).

In the friction limited case the length and diameter of the capillary becomes important. The flow is treated as adiabatic, but it is not isentropic, i.e. adiabatic and frictionless, any more, since friction increases the entropy.

Dependent on the diameters D_v of the valve, D_p of the capillary, the capillary length and a surface friction factor (cf.[15]), one can detect the flow limiting element as big capillaries attached to small orifices may have no influence on the gas flux. Then the exact capillary length and diameter does not play a role.

In[15] it is shown a way to calculate the critical diameter $D_{p,\mathrm{trans}}$ for which the capillary becomes the flux limiting element.

- If $D_{p,\mathrm{trans}} \leq D_p$, the tube does not limit the particle flux so that Equation 8 is used to describe the system.
- If $D_{p,\mathrm{trans}} > D_p$, a set of parametric equations as described in[15] has to be used to calculate the resulting gas flux.

Figure 3 shows that the orifice diameter is fixed to $D_v = 400\,\mu\mathrm{m}$, independent of the attached capillary diameter. Following[15] to solving the set of parametric equations leads to

$$D_{p,\mathrm{trans}} = 760\,\mu\mathrm{m}. \tag{10}$$

For bigger or removed capillaries only the thinnest part in the nozzle with $D_v = 400\,\mu\mathrm{m}$ limits the flowrate. Figure 7 shows that the 700 µm capillary slightly decreases the flowrate, since the friction limited regime becomes dominant.

VI. RESULTS: MEASURED FLOWRATE

In this section, the actual properties of the valve are explored and discussed. We will start with the flow rate dependence on the Piezo voltage, continue with the role of nozzle diameter and length for various pressures as well as the influence of the temperature on the valve properties. Before doing so, the measurement uncertainties are discussed: The errorbars of the measurement include the following uncertainties:

- Volume of the vacuum chamber $\pm 5\,\mathrm{l}$.
- Temperature of the vessel $\pm 2\,\mathrm{K}$.
- Baratron absolute $\pm 1 \times 10^{-2}\,\mathrm{Pa}$, relative $\pm 1\,\%$
- Error in gas filling pressure of $\pm 15\,\mathrm{mbar}$ for $p > 1\,\mathrm{bar}$ and $\pm 2\,\mathrm{mbar}$ for $p < 1\,\mathrm{bar}$.

For all measurements, helium was used as working gas.

A. Voltage regulation

Figure 6, shows the gas flux as a function of the piezo voltage for three different filling pressures (helium). For a voltage $U < U_{\mathrm{open}}$ the valve is closed. The value of U_{open} depends on the initial tension of the sealing. For $U_{\mathrm{open}} < U < U_{\mathrm{sat}}$, the flux is limited by the distance of the sealing point to the Viton element.

A simple estimation of the necessary distance for a full opening can be achieved by equalising

the orifice cross section with the shell area of a hypothetical cylinder. This cylinder has the same ground area as the orifice, its height is defined as the distance of the Viton element to the orifice. This leads to a minimum distance of 0.25 times the diameter of the orifice for a full opening of a valve. For the 400 µm sealing perforation this gives a minimal distance of 100 µm.
For $U > U_{\mathrm{sat}}$ the gas flux is limited by the capillary (or the orifice diameter) and does not change with the voltage.
The opening and saturation voltage as well as the shape of the curves stay constant for all pressures. The level of saturation is dependent on the pressure as shown in Figure 7.
The voltage span between U_{open} and U_{sat} depends on the stiffness of the system which is much higher for the Viton plate sealing. Figure 6 shows that this voltage span for the Viton plug a) is 30 V compared to 10 V for the Viton plate b). The smaller voltage span needed for a full opening decreases the switching time for the Viton plate sealing b) by a factor of 3 compared to the Viton plug a).

The slope at the steepest point of the curve for 1000 mbar in Figure 6 a) is $(6.9 \pm 0.4) \times 10^{19}$ pps/V. 1 V piezo voltage corresponds to a distance change of 4.77 µm. This shows that small changes in the geometry (e.g. relaxation of the Viton plug and oscillations) have an enormous influence on the flowrate in this region.
For a more robust behaviour of the valve it is therefore recommended to use the maximal piezo voltage, yielding a complete opening of the valve and to regulate the gas flow by pressure variation at a rate of $(1.333 \pm 0.015) \times 10^{18}$ pps/mbar for the 700 µm capillary (cf. Section VI B).

B. Pressure variation

Variation of the pressure at fully opened valve has shown to be the most precise way to regulate the gas flux. As shown in Figure 7, for sufficiently high pressures, the dependence of the flowrate on the pressure is linear and can be described by Equation 8. The regression

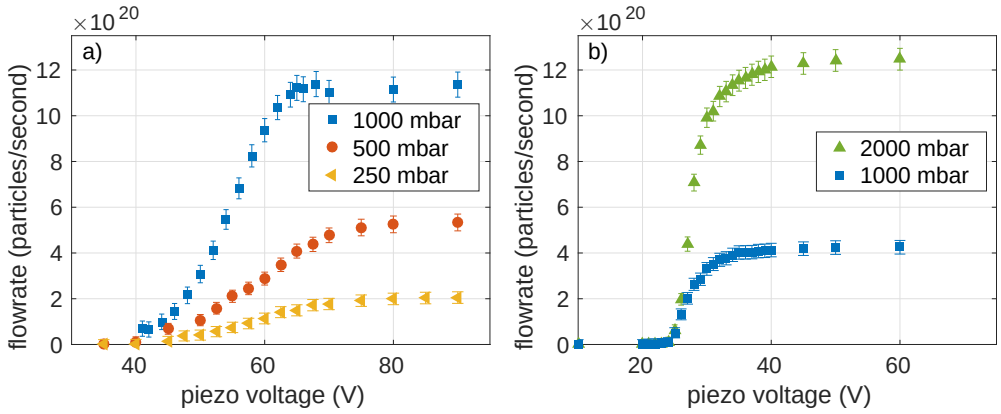

FIG. 6: Voltage dependent gas flux for different pressures. a) Viton plug sealing with 700 µm capillary, b) Viton plate sealing with 400 µm capillary.

leads to

$$\begin{aligned}
\dot{N}(p)|_{298\,\mathrm{K,no\,cap.}} &= (1.635 \pm 0.003) \times 10^{18}\ \dot{N}/\mathrm{mbar} \cdot p - \\
&\quad (5.2 \pm 1.6) \times 10^{19}\ \dot{N} \\
\dot{N}(p)|_{298\,\mathrm{K,700\,\mu m}} &= (1.333 \pm 0.015) \times 10^{18}\ \dot{N}/\mathrm{mbar} \cdot p - \\
&\quad (1.5 \pm 0.3) \times 10^{20}\ \dot{N} \\
\dot{N}(p)|_{298\,\mathrm{K,400\,\mu m}} &= (7.66 \pm 0.12) \times 10^{17}\ \dot{N}/\mathrm{mbar} \cdot p - \\
&\quad (2.9 \pm 0.5) \times 10^{20}\ \dot{N}
\end{aligned}$$

where $\dot{N}$ is the particle flowrate per second and p is the gas pressure (He) in mbar.
The theoretical descriptions of the flowrates (cf. Section VI) achieves an excellent agreement with the measured slope of the linear pressure dependence. This is shown in Figure 7 for three different cases. However, it is necessary to set a friction factor (cf.[15]) within the solving process which is hard to determine exactly and strongly depends on the chosen capillary. In contrast to the measurements, Equation 8, which describes the gas flow through an orifice, does not predict an offset for the linear regime. However, this is reasonable, since the dependence becomes quadratic for low pressures, where compressible effects become negligible due to smaller pressure differences. Figure 8 shows that the smaller capillary limits the expansion by frictional processes and hence reduces the pressure gradient which leads to a wider range of quadratic dependence. Without attached capillary the quadratic regime nearly vanishes, since in this case the flux is limited by the orifice diameter, leading to strong pressure gradients (cf. Section V B). This is confirmed by the increasing offset of

the linear function the more the flow gets friction limited. This offset is demonstrated in Figure 7 for the thinnest capillary by comparing the theory curve (dashed line) which goes through zero with the offset corrected theory values.

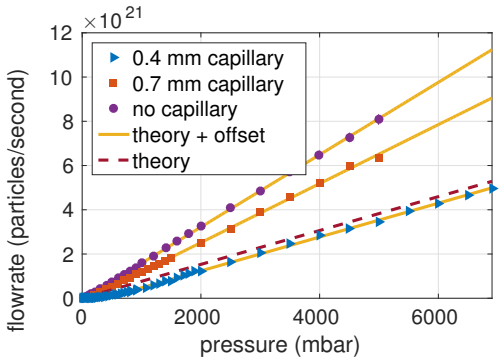

FIG. 7: Pressure dependent gas flux for two different capillary diameters and without attached capillary.

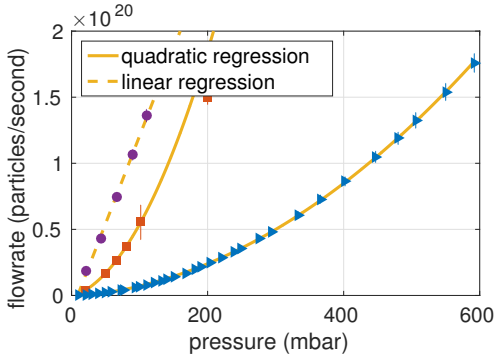

FIG. 8: Magnification of the low pressure regime from Figure 7, the symbols following the previous notation. For the 400 µm capillary, the flux regime with a quadratic pressure dependence is valid for higher pressures, compared to the 700 µm capillary. With no capillary attached to the sealing point, the flow regime is linear for all measured pressures.

C. Temperature variation

Although the flowrate of the valve is not directly affected by temperature changes (within the operation limits), the opening process of the valve is temperature dependent. The main reason is that the total stroke of the piezo actor decreases with increasing temperature ($\sim (4.0 \pm 1.5)\,\mu m/K$ for $25\,^{\circ}C < T < 80\,^{\circ}C$). Also the thermal expansion of Viton reduces

the effective opening at higher temperatures, mainly for the Viton pulg sealing.
Both lead to a shift of the opening voltage U_{open} to higher values with rising temperature as presented in Figure 9 a) for the Viton plug sealing and in b) for the Viton plate sealing, where the voltage dependent flowrate has been measured for different temperatures.
The sealing concept based on the Viton plate shows a better behaviour, here the valve can be opened fully at maximum operation temperature.

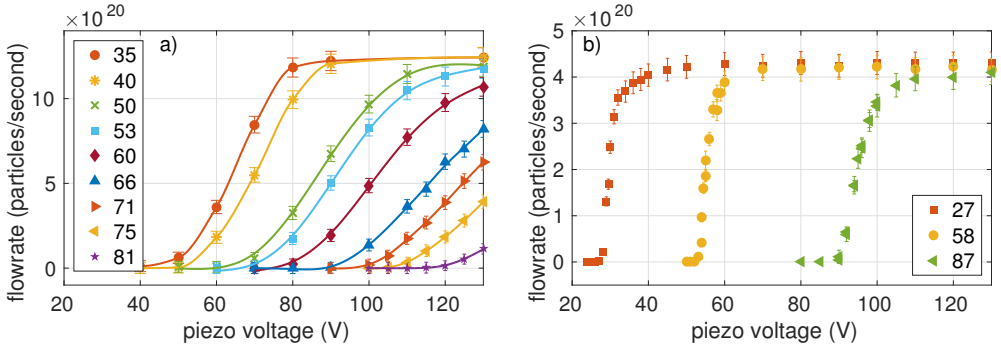

FIG. 9: Voltage dependent flowrate for different temperatures in °C. a) shows the temperature dependence for the viton plug sealing (lines to guide the eye) whereas b) shows the temperature behaviour of the viton plate sealing type.

D. Gas type dependency

The gas flux through a valve is dependent on the gas type as can be seen in Equation 6 with the gas dependent quantities c_s and γ, where the dominant effect is mostly the $1/\sqrt{m}$ dependence of the adiabatic sound speed c_s. To demonstrate this influence we have compared helium to other gases as argon, nitrogen (N_2) and deuterium (D_2) which are also common gases used in fusion applications for diagnostic and fuelling.
The flux reduction of the heavier gases argon and nitrogen, compared to helium is plotted in Figure 10, measured with the 700 µm capillary.

For deuterium, the flux difference to helium is not as pronounced as both gases have the same mass. In contrast to helium, the nature of deuterium is a two atomic molecule with two additional degrees of freedom. So the ratio of specific heat is with $\gamma_{D_2} = 7/5$ lower than for helium with $\gamma_{He} = 5/3$. The dependence of the flowrate on γ, as it is given by Equation 8, is quite complex, although the square root behaviour dominates. So, the flowrate is by 5.7 %

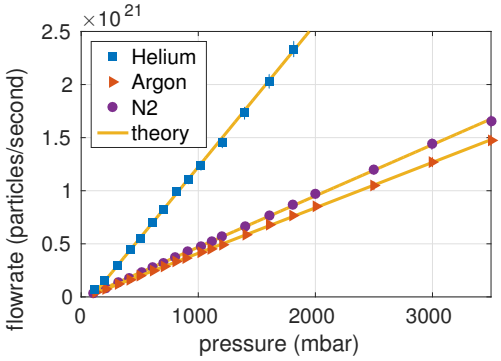

FIG. 10: Dependency of the flowrate on the gas type for the two noble gases helium and argon as well as for nitrogen (N_2). Measured with the 700 µm capillary.

lower for deuterium.

All measurement results are compared to the theoretical prediction in Table I. As the measured result are in excellent agreement with the theoretical prediction of the flux reduction, the table is supplemented for additional gases often used in fusion research. The flux changes listed in the table are referred to helium as this is the working gas used in this paper.

TABLE I: Influence of the gas type on the achievable flux, compared to helium.

	unified		flux change (percent)	
gas type	atomic mass	γ	measured	theory
helium	4	5/3	0	0
hydrogen	2	7/5	–	+33.3
deuterium	4	7/5	-4.1 ± 1.5	−5.7
neon	20.18	5/3	–	−55.5
nitrogen	28	7/5	-64.1 ± 0.3	−64.4
argon	39.95	5/3	-68.2 ± 0.2	−68.4

VII. SWITCHING TIMES

One advantage of the chosen valve design is the ability of the fast modulation of thermal gas beams. To realise this, the piezo element, which behaves like a capacitor, has to be charged and discharged quickly.

A suitable piezo driver is the system "30V300"[17], which provides a maximum current of 300 mA, leading to a switching time of 3.1 ms for a full opening of the piezo from −20 V to 130 V.

Figure 11 shows the piezo voltage as a function of time after the control signal change. The piezo voltage is proportional to the expansion of the piezo ceramic whereas the total movement of the piezo actor corresponds to the ceramic movement amplified by a spring system surrounding the ceramic (stiffness: 0.06 N/µm).

The total movement of the actor has been traced with a fast camera (model "Phantom v711"[18]). The resulting trajectory, plotted in Figure 11 (blue), shows that the piezo movement closely follows the applied voltage (yellow). The delay between the start of the movement and the trigger is caused by the initial tension of the piezo-spring system as well as the elasticity of the Viton plate. The main part of the piezo movement begins at the point when the Viton plate detaches from the orifice at around 40 V piezo voltage (dependent on the initial tension, cf. Figure 6). At 3.1 ms the piezo is fully charged with 120 V, corresponding to a stroke of 500 µm. Inertia causes an overshooting of the piezo of about 180 µm, leading to a damped oscillation with the resonance frequency of 250 Hz. This resonance frequency depends on the movable mass connected to the piezo. In this case the sealing mechanism leads to a load of 2.84 g.

For the operation with fully opened piezo valve this oscillation is not influencing the particle flux because the minimal distance during oscillation between the sealing plate and the orifice is always larger than the maximal distance (100 µm, cf. Section VI A) limiting the particle flux.

The buildup time of the injected gas beam is even faster than the full opening time of the piezo from −20 V to 130 V. This can be seen in Figure 6 a) where only the voltage change between 40 V and 70 V influences the gas flux. This reduces the relevant time by 80 %. With the Viton plate as sealing mechanism, the system is more stiff so that only a voltage change of 10 V is required for a full opening (cf. Figure 6 b)), leading to gas formation times < 0.5 ms. An experimental proof for the fast buildup of the thermal beam is the temporally resolved measurement of the emission intensity of a helium beam injected into a glow discharge, measured with a fast camera. Figure 12 shows that the emission intensity rises within 300 µs to a plateau value.

Thus, sharp gas pulses with short interruptions for background subtraction can be produced as shown in section IX.

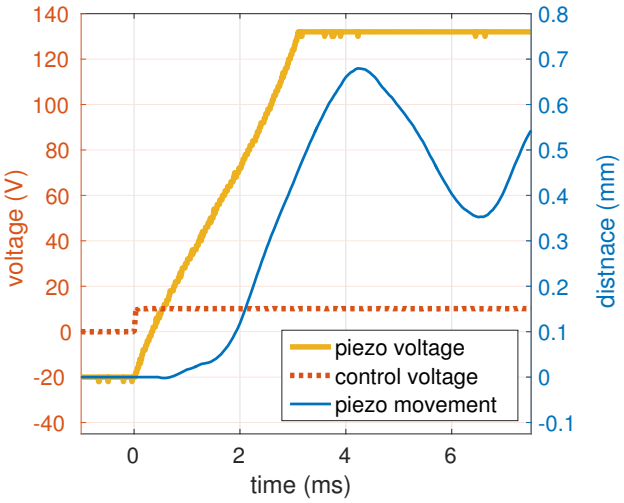

FIG. 11: Switching time of the piezo valve. Plotted is the total movement of the sealing plate (blue) compared to the piezo voltage (yellow) as a function of time together with the control signal (red).

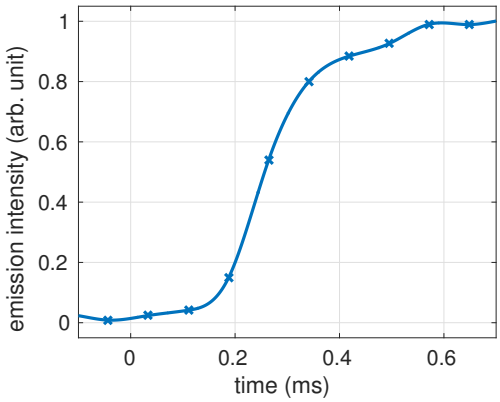

FIG. 12: Emission of helium injected into a glow discharge. The rise time of 300 µs shows the fast response of the valve.

VIII. GAS CLOUD SHAPE

To measure the beam geometry, the valve is placed in a helium glow discharge, current controlled at 500 mA and a background pressure of 4×10^{-4} mbar.

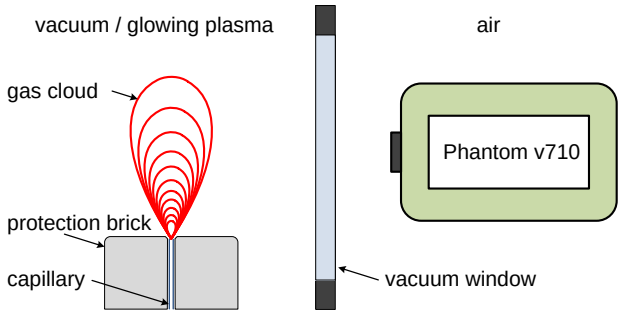

FIG. 13: Scheme of the optical measurement of the gas distribution and emission rise time. The fast camera "Phantom v710" was used with a frame rate up to 10 000 Hz.

When additional helium or other gases are injected into the glow discharge by the piezo valve, the injected neutral gas is excited mainly by the plasma electrons and therefore emits light. This emission is brighter than the homogeneously emitted light of the glow discharge, due to the higher local gas density.

As shown in Figure 13, a fast camera (model "Phantom v710") was used to measure the total line integrated 2D emission intensity. The result of such a measurement can be seen in Figure 14 for injected deuterium after background subtraction. It has to be remarked that an inverse Abel Inversion is not necessary to reconstruct the 3D emission distribution from the measured line integrated data in case of a Gaussian emission profile.

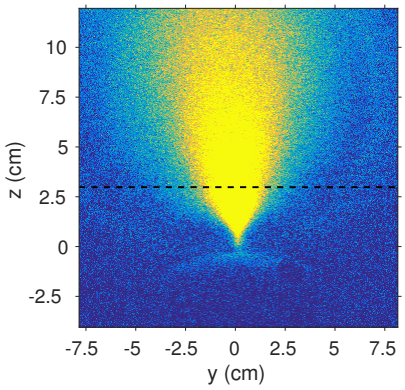

FIG. 14: Emission of a deuterium gas cloud, excited by a helium glow discharge plasma after background subtraction. A cross section profile is presented in Figure 15 for the dashed line.

We can assume a symmetric 2D Gaussian distribution (cf. Figure 15) of the gas density

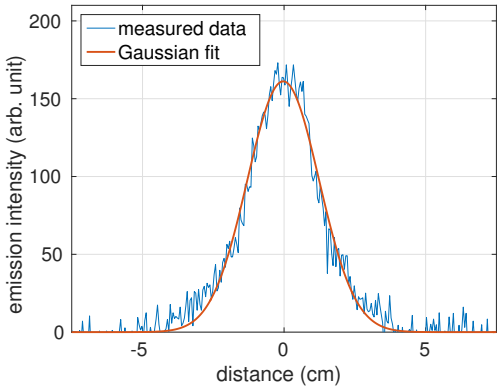

FIG. 15: 1D Emission profile at 3 cm distance to the valve.

$n(x, y, z)$ in planes perpendicular to the capillary which is aligned in the z-direction.

$$n(x, y, z) = \frac{1}{2\pi\sigma(z)^2} \cdot \exp\left(-\frac{x^2 + y^2}{2\sigma(z)^2}\right) \tag{11}$$

The gas expands in a cone shaped cloud, where the radius of the cone (dependent on the distance to the injection point) is defined as the Full Width Half Maximum (FWHM) of the Gaussian distribution. It is given by

$$\text{FWHM} = 2\sigma\sqrt{2\ln 2}. \tag{12}$$

The FWHM increases linearly with rising distance like

$$\text{FWHM} = 2z \cdot \tan\alpha, \tag{13}$$

where α is the half angle of beam spread. Combining Equation 12 and Equation 13 leads to the relation

$$\sigma(z) = \frac{z \cdot \tan\alpha}{\sqrt{2\ln 2}}. \tag{14}$$

To evaluate the measured data in order to calculate the angle of beam spread 2α, Gaussian functions were fitted to the background subtracted camera data line by line. The FWHM of each line were combined for all distances z to the nozzle as long as the fit was good enough ($R^2 > 0.92$, cf. Figure 16). A linear fit through the data gives $\tan\alpha$ (cf. Equation 13). Table II shows the angle of beam spread α for three different gas types.

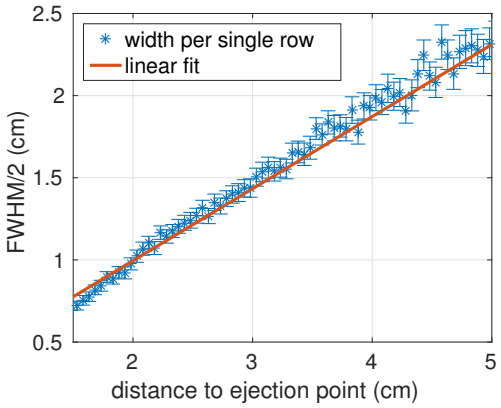

FIG. 16: Width of the single Gaussian fits for different distances to the gas injection point.

TABLE II: Comparison of the half angle of beam spread α for different combinations of gas type and pressure.

gas type	pressure (mbar)	α (degree)
helium	5000	20.0 ± 1.5
deuterium	600	25.4 ± 0.5
argon	400	18.9 ± 0.5

IX. APPLICATION PROSPECTS

Active spectroscopy is a powerful tool to obtain local plasma parameters from the edge of high temperature plasmas. Locally injecting small amounts of suitable gases into the plasma enables high local emission intensities and facilitates high spatial resolution for the measurement.

Two of the presented piezo valves had been installed in ASDEX Upgrade (AUG)[19] and were successfully tested with over 1000 cycles for gas-puff imaging[8] and line ratio spectroscopy on helium[4]. A further application is planned for thermal charge exchange recombination spectroscopy (CXRS) on non fully ionised impurities in the scrape-off layer.

Another piezo system with a cascade of five inlet tubes is implemented in the stellerator W7-X in Greifswald[20] used as thermal helium beam[21] and fuelling valve as well as for impurity transport studies[22].

As application example we present measurements from the newly implemented thermal helium beam diagnostic at AUG which uses line ratio spectroscopy on injected helium to

determine the electron temperature and density in the scrape-off-layer (SOL). For this purpose the piezo valve was operated with 50 mbar helium (700 µm capillary, fully opened). Gas puffs of 50 ms duration were injected into the plasma leading to a particle flux of 1.68×10^{19} part/s during the pulses. With a thermal beam velocity of 1.24 km/s local helium densities of 2×10^{18} /m^3 had been achieved at the measurement point in a distance of 6.5 cm to the gas ejection point, corresponding to a normalised poliodal flux radius of $\rho_{\mathrm{pol}} = 1.05$.
The high neutral densities of helium, injected with the presented piezo system, led to a strong emission of light in a radial region of around 7 cm in AUG plasmas, making the thermal helium beam accessible in regions corresponding to $0.98 < \rho_{\mathrm{pol}} < 1.06$.

Figure 17 shows the timetrace of the AUG discharge #32 032, where 50 He puffs had been injected into the plasma. The helium gas flux during the puffs is around 600 times less than the continuously injected deuterium for plasma fuelling.
The discharge starts in the low confinement mode (L-mode) with a transition to the high confinement mode (H-mode) at ~ 3 s by switching on the neutral beam heating P_{NBI}. The edge localised modes (ELMs) appearing in H-mode are indicated with the divertor shunt current $I_{\mathrm{i-DIV}}$. ELMs are very sensitive to perturbations of the plasma edge region. However the ELM behaviour does not change during the He puffs which is an indicator for the undisturbed plasma edge region during the operation of the piezo valve with low helium fluxes.
The lowest plot in Figure 17 shows the emission timetrace of the helium 667.8 nm line at two radial positions. The smaller radius lies in the confined region of the plasma, whereas the larger radius is dedicated to the outer SOL, close to the gas injection point. It is to remark that the emission in L-Mode is highest in the confined region of the plasma ($R = 2.12$ m), although the neutral helium density is higher in the far SOL ($R = 2.16$ m). The reason therefore is the more efficient excitation of the helium for higher plasma temperatures. In H-mode this effect becomes compensated by the increasing amount of ionisation of the injected helium in the confined region on the one hand and by the increasing plasma temperature in the SOL on the other hand.
A zoom of this emission timetrace is shown in Figure 18 for three helium puffs in the L-Mode. The absolute emission of the injected helium is measured along lines of sight tangential to the flux surface and resolved with a grating spectrometer equipped with a fast CCD camera

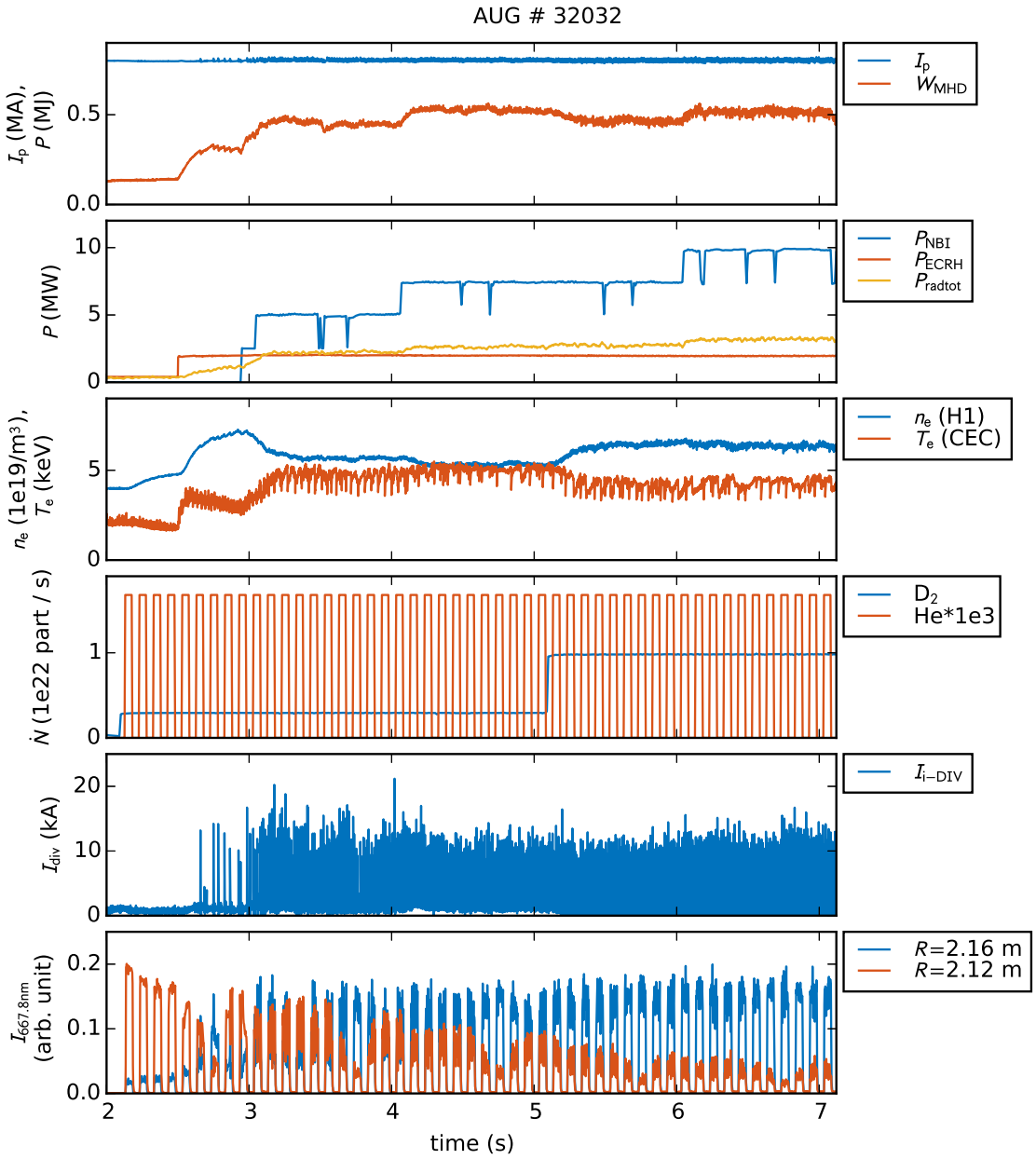

FIG. 17: Experimental timetrace of AUG discharge #32 032. The timetrace show the plasma current I_{P}, the total stored energy in the plasma W_{MHD}, the neutral beam injection and electron cyclotron resonance heating power P_{NBI} and P_{ECRH}, the total radiated power P_{radtot}, the line integrated electron density n_{e} and core electron temperature T_{e}, the total plasma fuelling with D_2 compared to the diagnostic He inlet, the shunt current of the inner divertor $I_{\mathrm{i-DIV}}$, denoting a L-H-transition at $\sim 3\,\mathrm{s}$ and the measured emission $I_{667.8\mathrm{nm}}$ at 667.8 nm of the injected helium at two radial positions.

(cf.[7] and[23]).

The temporal resolution is limited in this case by the CCD camera to 2.3 ms, nevertheless the short rise and decay time of the helium emission can be verified. This demonstrates successfully the application of the fast piezo valve for diagnostic purposes, especially when fast offset substraction is required.

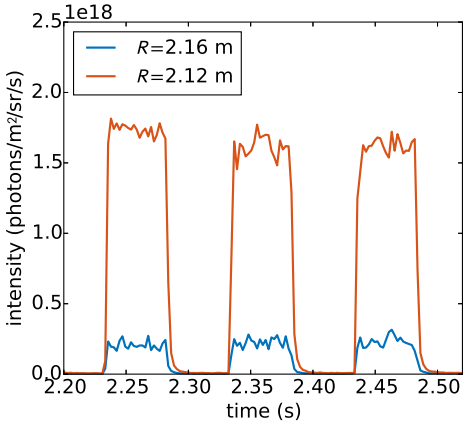

FIG. 18: Measured intensity time trace of the absolute emission of the helium 667.8 nm during three helium gas puffs in the AUG discharge #32 032 at a poloidal radius of $\rho_{\mathrm{pol}} = 1.05$ in the far scrape-off layer and $\rho_{\mathrm{pol}} = 0.99$ in the confined region close to the separatrix.

The impact of the pulsed driven piezo valve with a helium flux of 1.68×10^{19} part/s on the absolute helium content in the plasma of AUG can be measured in the confined region with charge exchange spectroscopy[24].

Figure 19 shows the absolute helium concentration during ten helium puffs at AUG discharge #32 167 at three different radial positions (toroidally close to the helium injection point). Whereas at the outer most position the single helium puffs are directly visible, the puffs lead only to a slight increase of the helium concentration in the plasma core ($\rho_{\mathrm{pol}} = 0.2$) in the order of 0.1 %.

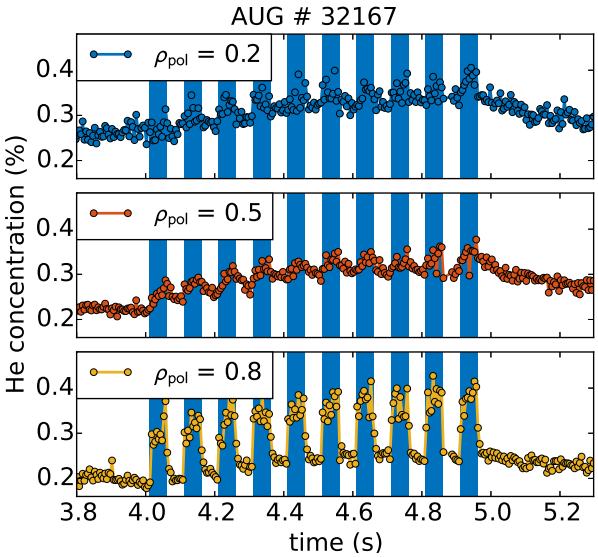

FIG. 19: Absolute helium concentration at three different radial positions in the confined region of the plasma. Measured with the helium charge exchange recombination spectroscopy at AUG discharge #32 167 for ten 50 ms He puffs with 1.68×10^{19} part/s.

X. SUMMARY

We presented a versatile gas injection system for the injection of thermal gas beams into vacuum chambers. It is based on a piezo element used to lift a Viton plate which is pressed on a perforated truncated cone for the normally closed valve. The gas expands through a thin capillary with selectable diameter and expands in a cone shaped gas beam with an half opening angle of about 20° for helium.

Dependent on the filling pressure of the valve from 10 mbar up to 100 bar and the chosen capillary diameter, gas fluxes are accessible from 10^{18} part/s up to 10^{23} part/s. The valve offers high duty cycles and fast switch on/off times of $\lesssim 0.5$ ms.

As the compact system withstands the harsh environment of fusion devices, it can be placed directly inside the vacuum chamber close to the plasma periphery. This makes the piezo valve an excellent device to provide gas injection for fuelling or diagnostic purposes as shown in the example of the thermal helium beam at ASDEX Upgrade.

ACKNOWLEDGMENTS

The versatile gas injection system was developed at FZ Jülich GmbH, Institut für Energie- und Klimaforschung - Plasmaphysik, Partner of the Trilateral Euregio Cluster (TEC), 52425 Jülich, Germany. It was modified, improved and implemented at ASDEX Upgrade by IPP Garching.

This work was funded in part by the U.S. Department of Energy under Grant DE-SC00013911 and DE-SC0014210.

This work has been carried out within the framework of the EUROfusion Consortium and has received funding from the Euratom research and training programme 2014-2018 under grant agreement No 633053. The views and opinions expressed herein do not necessarily reflect those of the European Commission.

REFERENCES

[1]S. C. Bates and K. H. Burrell, Review of Scientific Instruments **55**, 934 (1984).

[2]M. Dibon, K. Mank, G. Pautasso, M. Griener, A. Herrmann, V. Mertens, R. Neu, B. Ploeckl, and V. Rohde, under review: Review of Scientific Instruments (2016).

[3]U. Kruezi, H. Stoschus, B. Schweer, G. Sergienko, and U. Samm, Review of Scientific Instruments **83**, 065107 (2012).

[4]O. Schmitz, I. L. Beigman, L. A. Vainshtein, B. Schweer, M. Kantor, A. Pospieszczyk, Y. Xu, M. Krychowiak, M. Lehnen, U. Samm, and B. Unterberg, Plasma Physics and Controlled Fusion **50**, 115004 (2008).

[5]R. Fischer, E. Wolfrum, and J. Schweinzer, Plasma Physics and Controlled Fusion **50**, 085009 (2008).

[6]M. Willensdorfer, E. Wolfrum, R. Fischer, J. Schweinzer, M. Sertoli, B. Sieglin, G. Veres, and F. Aumayr, Review of Scientific Instruments **83** (2012), 10.1063/1.3682003.

[7]E. Viezzer, T. Pütterich, R. Dux, and R. McDermott, Review of Scientific Instruments **83**, 103501 (2012).

[8]G. Fuchert, G. Birkenmeier, D. Carralero, T. Lunt, P. Manz, H. W. Müller, B. Nold, M. Ramisch, V. Rohde, and U. Stroth, Plasma Physics and Controlled Fusion **56**, 125001 (2014).

[9]Piezosystem Jena GmbH, Stockholmer Straße 12, 07747 Jena, Germany.

[10]Technetics Group, Falkenweg 1, 41468 Neuss, Germany.

[11]LEMO Elektronik GmbH, Hanns-Schwindt-Str. 6, 81829 München, Germany.

[12]R. W. Johnson, *Handbook of Fluid Dynamics*, Handbook Series for Mechanical Engineering (Taylor & Francis, 1998).

[13]W. Demtröder, *Experimentalphysik 1: Mechanik und Wärme*, 4th ed. (Berlin, Heidelberg, New York, 2008) p. 513.

[14]A. H. Shapiro, "The Dynamics and Thermodynamics of Compressible Fluid Flow," (1953), arXiv:9710089v2 [gr-qc].

[15]P. Parks and W. Wu, Nuclear Fusion **51** (2011), 10.1088/0029-5515/51/7/073014.

[16]U. Kruezi, *Entwicklung einer Heliumstrahldiagnostik zur Messung der Elektronendichte und -temperatur mit hoher räumlicher und zeitlicher Auflösung*, Dissertation, Heinrich-Heine-Universität Düsseldorf (2006).

[17]Piezosystem Jena GmbH, Stockholmer Straße 12, 07747 Jena, Germany.

[18]Vision Research, 100 Dey Road, Wayne, New Jersey 07470, USA.

[19]H. Zohm, J. Adamek, C. Angioni, G. Antar, C. Atanasiu, M. Balden, W. Becker, K. Behler, K. Behringer, A. Bergmann, T. Bertoncelli, R. Bilato, V. Bobkov, J. Boom, A. Bottino, M. Brambilla, F. Braun, M. Brüdgam, A. Buhler, A. Chankin, I. Classen, G. Conway, D. Coster, P. de Marné, R. D'Inca, R. Drube, R. Dux, T. Eich, K. Engelhardt, B. Esposito, H.-U. Fahrbach, L. Fattorini, J. Fink, R. Fischer, A. Flaws, M. Foley, C. Forest, J. Fuchs, K. Gál, M. G. Muñoz, M. G. Adamov, L. Giannone, T. Görler, S. Gori, S. D. Graça, G. Granucci, H. Greuner, O. Gruber, A. Gude, S. Günter, G. Haas, D. Hahn, J. Harhausen, T. Hauff, B. Heinemann, A. Herrmann, N. Hicks, J. Hobirk, M. Hölzl, D. Holtum, C. Hopf, L. Horton, M. Huart, V. Igochine, M. Janzer, F. Jenko, A. Kallenbach, S. Kálvin, O. Kardaun, M. Kaufmann, M. Kick, A. Kirk, H.-J. Klingshirn, G. Koscis, H. Kollotzek, C. Konz, K. Krieger, T. Kurki-Suonio, B. Kurzan, K. Lackner, P. Lang, B. Langer, P. Lauber, M. Laux, F. Leuterer, J. Likonen, L. Liu, A. Lohs, T. Lunt, A. Lyssoivan, C. Maggi, A. Manini, K. Mank, M.-E. Manso, M. Mantsinen, M. Maraschek, P. Martin, M. Mayer, P. McCarthy, K. McCormick, H. Meister, F. Meo, P. Merkel, R. Merkel, V. Mertens, F. Merz, H. Meyer, A. Mlynek, F. Monaco, H.-W. Müller, M. Münich, H. Murmann, G. Neu, R. Neu, J. Neuhauser, B. Nold, J.-M. Noterdaeme, G. Pautasso, G. Pereverzev, E. Poli, S. Potzel, M. Püschel, T. Pütterich, R. Pugno, G. Raupp, M. Reich, B. Reiter,

T. Ribeiro, R. Riedl, V. Rohde, J. Roth, M. Rott, F. Ryter, W. Sandmann, J. Santos, K. Sassenberg, P. Sauter, A. Scarabosio, G. Schall, H.-B. Schilling, J. Schirmer, A. Schmid, K. Schmid, W. Schneider, G. Schramm, R. Schrittwieser, W. Schustereder, J. Schweinzer, S. Schweizer, B. Scott, U. Seidel, M. Sempf, F. Serra, M. Sertoli, M. Siccinio, A. Sigalov, A. Silva, A. Sips, E. Speth, A. Stäbler, R. Stadler, K.-H. Steuer, J. Stober, B. Streibl, E. Strumberger, W. Suttrop, G. Tardini, C. Tichmann, W. Treutterer, C. Tröster, L. Urso, E. Vainonen-Ahlgren, P. Varela, L. Vermare, F. Volpe, D. Wagner, C. Wigger, M. Wischmeier, E. Wolfrum, E. Würsching, D. Yadikin, Q. Yu, D. Zasche, T. Zehetbauer, and M. Zilker, Nuclear Fusion **49**, 104009 (2009).

[20]M. Krychowiak, J. Baldzuhn, B. Blackwell, T. Barbui, C. Biedermann, H.-S. Bosch, S. Bozhenkov, T. Bräuer, B. Carvalho, W. Biel, B. Buttenschoen, G. Cseh, A. Czarnezka, F. Effenberg, M. Endler, L. Stephey, H. Thomsen, J. M. Travere, T. Szepesi, U. Wenzel, A. Werner, H. Schuhmacher, T. Windisch, R. Wolf, G. Wurden, D. Zhang, A. Zimbal, S. Zoletnik, A. Alonso, M. Beurskens, R. Brakel, C. Alvaro, and R. Burhenn, under review: Review of Scientific Instruments (2016).

[21]T. Barbui, M. Krychowiak, R. König, O. Schmitz, J. Munoz-Burgos, B. Schweer, and A. Terra, under review: Review of Scientific Instruments (2016).

[22]L. Stephey, G. A. Wurden, O. Schmitz, H. Frerichs, F. Effenberg, C. Biedermann, J. Harris, R. König, P. Kornejew, M. Krychowiak, and E. A. Unterberg, Review of Scientific Instruments **87**, 11D606 (2016).

[23]M. Cavedon, *Technische Universität München Max-Planck-Institut für Plasmaphysik The role of the radial electric field in the development of the edge transport barrier in the ASDEX Upgrade tokamak*, Ph.D. thesis (2016).

[24]Athina Kappatou, *Investigations of helium transport in ASDEX Upgrade plasmas with charge exchange recombination spectroscopy*, Ph.D. thesis (2014).